Deposition of Photocatalytic TiO₂ Coating by Modifying the Solidification Pathway in Plasma Spraying

Kui Wen [1,2] (ID)**, Min Liu** [1,2]**, Xuezhang Liu** [1,2,3,*] (ID)**, Chunming Deng** [2] **and Kesong Zhou** [1,2,*] (ID)

1. School of Materials Science and Engineering, Central South University, Changsha 410083, China; wenkui@csu.edu.cn (K.W.); liumin_gz@163.net (M.L.)
2. National Engineering Laboratory for Modern Materials Surface Engineering Technology, The Key Lab of Guangdong for Modern Surface Engineering Technology, Guangdong Institute of New Materials, Guangzhou 510651, China; denghans@126.com
3. School of Materials and Mechanical Engineering, Jiangxi Science and Technology Normal University, Nanchang 330013, China
* Correspondence: xuezhang_liu@126.com (X.L.); kszhou2004@163.com (K.Z.)

Abstract: The deposition of photocatalytic TiO₂ coatings with plasma spraying is attractive for large-scale applications due to its low cost and simplicity, but it is still a challenge to obtain a TiO₂ coating with high anatase content. The solidification pathway of inflight melted particles was investigated in the present paper, and TiO₂ coatings with enhanced photocatalytic activity were obtained without a significant loss of the microhardness. The coating microstructure, phase composition, and crystallite size were investigated by scanning electron microscopy (SEM) and X-ray diffraction (XRD). Photocatalytic performance was evaluated by decomposing an aqueous solution of methylene blue. Results showed that the anatase content in TiO₂ coating was augmented to 19.9% from 4%, and the time constant of the activity was increased to 0.0046 h^{-1} from 0.0017 h^{-1}.

Keywords: photocatalytic coatings; solidification; plasma spraying; TiO₂; microstructure

1. Introduction

Titanium dioxide (TiO₂) has been extensively investigated due to its high photocatalytic activity [1,2]. There are three normal crystal phases for TiO₂ material: brookite, anatase, and rutile. Under atmosphere pressure and temperature, rutile is the stable phase. Calcined at the temperature about 573 to 1073 K, anatase and brookite will irreversibly transform into rutile. However, the photocatalytic activity of rutile is lower than that of anatase due to an increased electron-hole recombination rate [3,4].

The deposition of TiO₂ coating well attached on the surface of a substrate can be more efficient and as compared to TiO₂ P25 powder or similar products, owing to the easy recovery of the photocatalyst from the water [5]. Several methods have been reported to prepare TiO₂ coatings, including vapor deposition [6,7], electrophoretic deposition [8,9], sol-gel [10], and thermal spraying [11]. In comparison to other methods, thermal spraying has several highlighted features to make it particularly attractive, which include flexibility and high efficiency.

Unfortunately, during the thermal spraying of a plasma jet with a temperature of 14,000 K, the powder feedstock is melted. These molten particles are then driven to deposit on a substrate. Compared with initial feedstock powders, the anatase transformation to rutile is clearly observed in sprayed coatings. Even given P25/20 TiO₂ granulated nanopowders as the starting powder, an anatase content of only 1.7%–5% were obtained in the coatings [12]. Then, retaining the metastable anatase phase in thermally sprayed TiO₂ coatings becomes a great challenge.

Bozorgtabar et al. [12] demonstrated that photocatalytic activity was strongly related to the process conditions of thermal spraying. Thus, Colmenares-Angulo et al. [13] adjusted spraying conditions to reduce the heat input, and expected to reduce the transformation of anatase TiO$_2$ to rutile. Ctibor et al. [14] reported that most of the reduced phases were formed in TiO$_2$ coatings. The stoichiometry was further found to be a function of process parameters. Zhang et al. [15] reported that oxygen vacancies at the surface remarkably prolonged the life of the photon-generated carrier. Thus, it significantly increased the activity. However, others have recently observed that oxygen vacancies caused a significant raise to the charge carrier recombination and resulted into a depressed photocatalytic activity [16].

Herein, modifying the solidification pathway of inflight melted particles was investigated by injecting distilled water into the plasma jet rather than adjusting the spray conditions, and photocatalytic TiO$_2$ coatings with enhanced activity were obtained. The elaborated coating microstructure was mainly characterized by SEM, while phase composition and crystallite size were investigated by XRD. Finally, the photocatalytic activity of the proposed TiO$_2$ coatings was evaluated by decomposing an aqueous solution of methylene blue.

2. Experimental

2.1. Atmospheric Plasma Spraying

An atmospheric plasma spraying system (MF-P1000, GTV, Luckenbach, Germany) was used to deposit TiO$_2$ coatings. A carrier gas with a flow rate of 3.5 L/min radially injected feedstock powder into the plasma jet, while distilled water was radially injected into the plasma jet through a nozzle with average diameter of 0.3 mm by a suspension feeder (GTV, Luckenbach, Germany). The powder injector was 8.0 mm apart from the gun outlet, while the solution injector was 15.0 mm away from the gun outlet. Three typical coatings were obtained with different feeding parameters. As seen in Table 1, the speed of the feed disc regulated the mass of the feedstock powder injected into the plasma jet, and the flow rate controlled the mass of distilled water injected into the jet.

Table 1. The details of plasma spraying parameters for TiO$_2$ coatings.

Spraying Parameters	Samples		
	TiO$_2$-12-0	TiO$_2$-12-30	TiO$_2$-20-30
Spraying current (A)	650	650	650
Spraying voltage (V)	69	69	69
Primary gas Ar (L/min)	40	40	40
Secondary gas H$_2$ (L/min)	10	10	10
Speed of feed disc (rpm)	1.2	1.2	2.0
Spraying distance (mm)	100	100	100
Flow rate (mL/min)	0	30	30

Micron-sized commercial TiO$_2$ powders ($-45 + 15$ μm, Sunspraying Science and Technology Co. Ltd., Beijing, China) were adopted as feedstock powders (Figure 1). Stainless steel plates (30 mm in diameter, STS316) were employed as substrates. Prior to the deposition, the substrates were cleaned with ethanol to remove contaminants, followed by blasting with Al$_2$O$_3$ abrasives.

2.2. Coating Characterization

Scanning electron microscopy (SEM, Nova-Nona-430, Thermo Fisher Scientific, Waltham, MA, USA) was utilized to investigate the microstructure of TiO$_2$ coatings. A UV-Vis spectrophotometer (HP8453, Agilent, Santa Clara, CA, USA) was used to record spectra in the wavelength range of 250 to 750 nm. Microhardness was obtained with a load of 100 g for 10 s using Vickers (2100B, Instron Tukon, Shanghai, China), and the value was averaged from five indents per specimen.

An X-ray diffractometer (XRD, D8-Advance, Bruker, Billerica, MA, USA) equipped with copper radiation X-ray was employed to assess the phase composition of the proposed coatings. The 2θ was acquired in the range of 20° to 90° with a 0.05° step size. The anatase content was simply determined by the use of the relationship given by Berger-Keller et al. [17]. Meanwhile, crystallite size was calculated using the Scherrer formula [18].
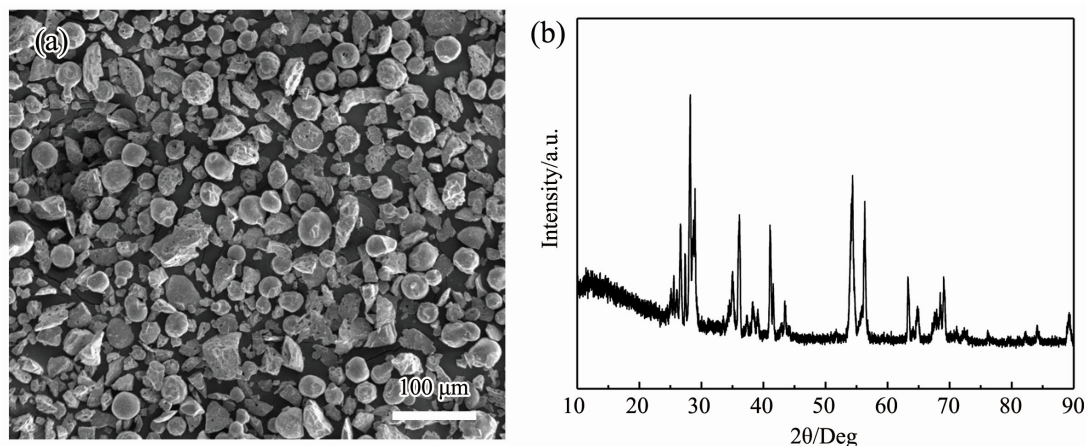

Figure 1. (**a**) SEM morphology and (**b**) XRD pattern of feedstock powders.

2.3. Photocatalytic Activity

The photocatalytic behavior of the TiO_2 coatings was assessed from decomposing methylene blue (MB) in a home-made setup. The coated samples were immersed in a glass reactor containing 50 mL of MB solution (5 ppm), and then illuminated with a UV-lamp ($\lambda = 370$ nm, $I = 2.5$ mW/cm^2). The concentration of MB was determined at certain intervals by measuring the solution absorbance with a UV-visible spectrometer at 664 nm wavelength, which was the maximum absorption peak of MB.

3. Results and Discussion

3.1. Crystal Structure and Phase Composition

The crystal structure and phase composition of as-deposited coatings were mainly analyzed by XRD. Figure 2 illustrates the patterns, where the dominant phase is rutile. The minor phase is anatase. It is interesting that there is some preferred orientation in XRD patterns. This may be resulted from the lamellar structure of as-deposited TiO_2 coatings stacked by flat granules, but it should be investigated further. Additionally, Ti_8O_{15} phases are observed in all of as-prepared samples, which is consistent with other works [13,19]. For TiO_2 coatings sprayed by thermal plasma, Magneli phases were widely reported [20]. This is mainly ascribed to the reduction of TiO_2, which results from the high temperature of the thermal plasma jet. There may be other reduced phases, but the analysis is inconclusive because the crystallite size is very small.

As shown in Figure 2, the peak intensity of 2θ = 25.25° (101) becomes stronger as distilled water is injected into the plasma jet. The XRD results illustrate that the total amount of anatase phase is increased by modifying the solidification pathway. Moreover, the anatase content and crystallite size are calculated by the Berger-Keller relationship and Scherrer formula, respectively. The results are demonstrated in Table 2.

At atmospheric pressure, anatase and brookite are two metastable phases. They can transform to rutile at the temperature range of 573–1073 K. However, from a thermodynamics view, the nucleation from the melt could be modified by the temperature and quenching rate [12]. Though anatase is a

metastable phase, it preferentially solidifies with a high quenching rate due to its lower surface energy in comparison to rutile ($\gamma_{Anatase}$ = 0.38 J·m^{-2}, γ_{Rutli} = 0.93 J·m^{-2}) [11,21].
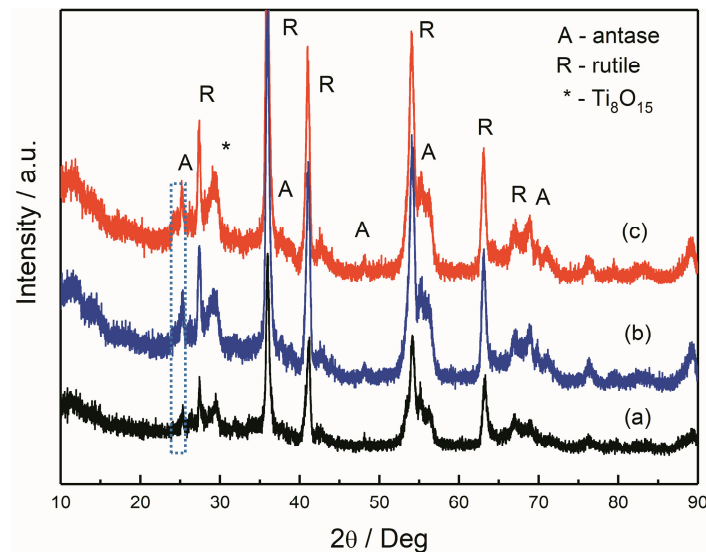
Figure 2. XRD patterns of TiO$_2$ coatings: (**a**) TiO$_2$-12-0, (**b**) TiO$_2$-12-30, and (**c**) TiO$_2$-20-30.

Table 2. Phase compositions and crystallites size of TiO$_2$ coatings.

Items	Samples		
	TiO$_2$-12-0	TiO$_2$-12-30	TiO$_2$-20-30
Anatase (Vol %)	4.0	11.0	19.8
Anatase crystallites average size (nm)	30.4	22.2	19.9
Rutile crystallites average size (nm)	73.0	40.2	27.0
Rate constant (h^{-1})	0.0017	0.0045	0.0046
R^2	0.9965	0.9966	0.9894

During the plasma spraying process, the plasma temperature is higher than 14,000 K. The speed can reach about 500 m/s [22]. TiO$_2$ particles are fully heated by the plasma jet. Consequently, these molten particles with high temperature deposit on the substrate. As the solidification temperature is close to the melting point of TiO$_2$, the particles are apt to nucleate into stable rutile. Therefore, the rutile phase (96%) in the coating is obtained, and the crystallite size is 73 nm.

However, when distilled water is injected into the plasma jet, the stream is fragmented into smaller drops and then evaporated. The evaporation of the droplet solvent can carry off a great deal of heat from melted particles, and those quenching particles with moderate temperature are deposited on the substrate. Thus, the particles solidify with the temperature lower than the melting point of TiO$_2$ and generate the anatase phase. As a result, the anatase content is 11% and 19.9% for TiO$_2$-12-30 and TiO$_2$-20-30, and the crystallite size is 22.21 and 19.9 nm.

3.2. Morphology Characterization

The photocatalytic performance of TiO$_2$ coatings is directly correlated to phase compositions and microstructural characteristics. Thus, the morphology and microstructure of TiO$_2$ coatings are investigated by SEM. The surface micrographs of TiO$_2$ coatings are shown in Figure 3. It can be observed that there is no significant discrepancy among these coated samples. They are all composed of fully molten areas and insufficient molten areas; the latter exhibit a rough surface. During the spraying process, the plasma jet of high enthalpy heats the injected particles and accelerates the melting to form solidified droplets (or splats) onto the substrate. Meanwhile, small voids are observed in

coating surface. This is mainly ascribed to un-melted particles. As a result, the pores and roughness can increase the reaction area between the catalyzer and the solution during the degradation of the MB dye.
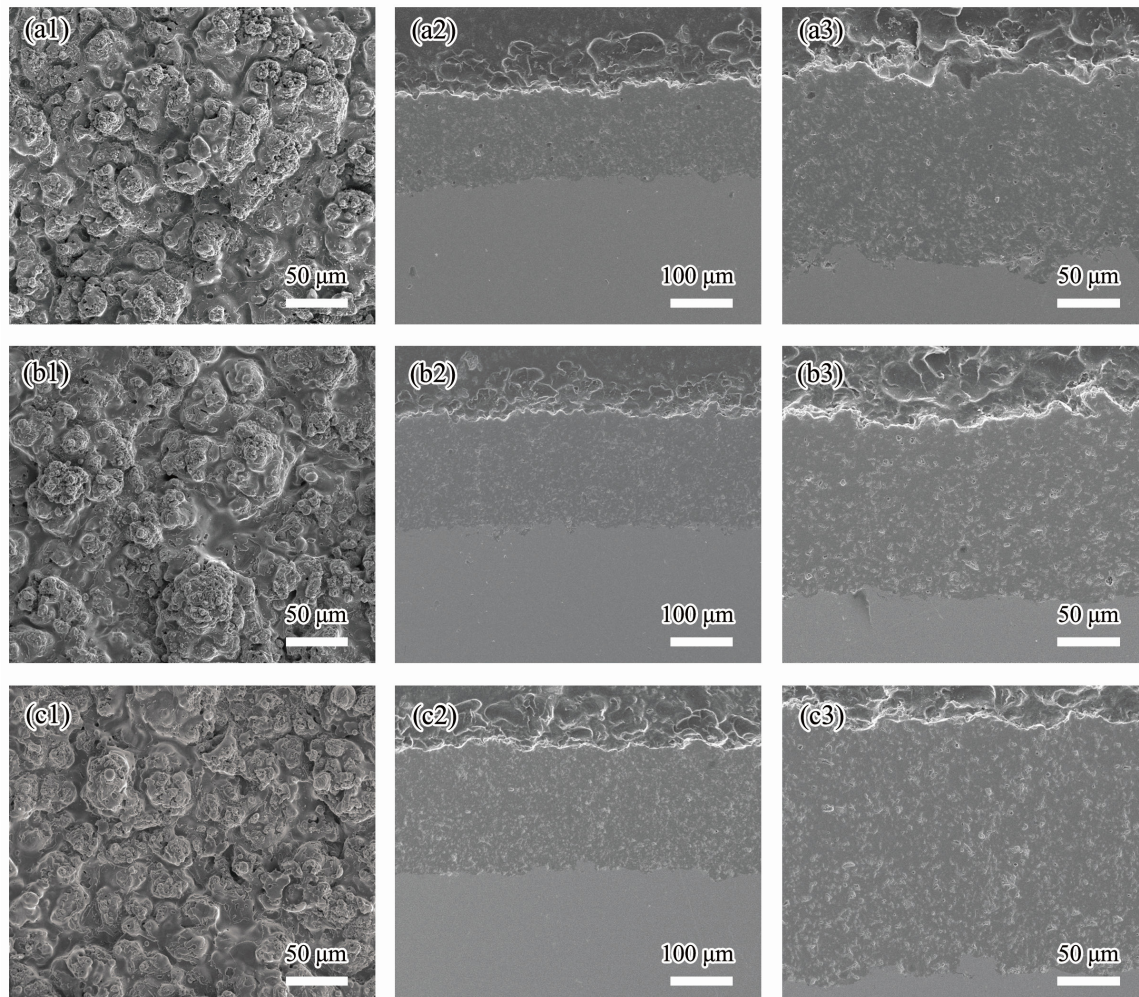

Figure 3. SEM images of TiO_2 coatings: (**a1–a3**) TiO_2-12-0, (**b1–b3**) TiO_2-12-30, and (**c1–c3**) TiO_2-20-30.

The corresponding cross-sections are illustrated in Figure 3 as well. Along with the morphology, those coatings all exhibit lamella structure. Meanwhile, the TiO_2 coatings are firmly bonded to the stainless steel substrates, and there is no crack at the interface. For the TiO_2-12-0 coating, some voids are observed, which may be resulted from the relaxation of the thermal stress of inter-laminar or incomplete contact between the plates and un-melted particles. When modifying the solidification pathway, the cross-section of the TiO_2-12-30 coating becomes fine and the porosity decreases obviously. On the other hand, the coating of TiO_2-20-30 presents a rough and porous cross-section that is caused by the lower melting point of the particles.

In addition, the thicknesses of TiO_2-12-0, TiO_2-12-30, and TiO_2-20-30 are about 150, 180, and 200 μm, respectively. The increased thicknesses of TiO_2-20-30 can be ascribed to the augmented speed of the feed disc (from 1.2 to 2.0 rpm). As the speed increases, more TiO_2 particles are injected into the plasma jet and take part in the coating deposition. However, it is interesting that the thickness of TiO_2-12-30 also becomes thicker when compared with TiO_2-12-0, because the speed of feed disc is 1.2 rpm. The results imply that distilled water injected into the plasma jet can not only modify the solidification pathway of inflight melted TiO_2 particles, but also can increase the deposition efficiency. Further study will be carried out to clarify this in future.

3.3. Microhardness

Functional coatings need sufficient mechanical properties and desired microstructures, while among the mechanical properties, the microhardness plays an important role on the long-term stability. Therefore, the influence of modifying the solidification pathway on the microhardness of TiO_2 coatings was reviewed.

The value of HV_{100} is 1148.27 for the TiO_2-12-0 coating. When adopting the modification, HV_{100} of the TiO_2-12-30 coating changes to 1137.8. This implies that there is no different discrepancy to the microhardness. With the modification, distilled water with a flow rate of 30 mL/min is radially injected into the plasma jet. The evaporation of water decreases the temperature of the plasma jet. However, the solution injector is 15.0 mm away from the gun outlet, which is located downstream of the powder injector, and thus the optimized injection does not violently affect the molten status of TiO_2 particles except those in the solidification pathway. Therefore, it does not cause a significant change to the microhardness.

However, the HV_{100} value slightly decreases to 1064.04 in the TiO_2-20-30 coating. The reason for this can be ascribed to the molten status of TiO_2 particles. As the speed of the feed disc increases from 1.2 to 2.0 rpm, more TiO_2 particles are injected into the plasma jet core. The temperature of the plasma jet already becomes lower with the modification of the solidification pathway, compared with TiO_2-12-0. Then, the heat energy shared by a single TiO_2 particle further decreases as more TiO_2 particles exist in the plasma jet, and some particles impact the substrate as un-melted or partially melted particles. As clarified in Figure 3(c2), this results in a rough and porous cross-section. Consequently, it slightly reduces the microhardness.

3.4. Photocatalytic Properties

The UV-Vis diffuse reflectance spectra of TiO_2 coatings were firstly recorded in the wavelength range of 250–750 nm. The results are illustrated in Figure 4. All coatings have an absorbance edge in the range of 390–400 nm, which is characteristic of semiconductor coatings. The absorbance edge is ascribed to the charge transfer from the valence band to the conduction band. For TiO_2 materials, the valence band is largely caused by $2p$ orbitals of the oxide anions, and the conduction band is constituted with $3d$ t_{2g} orbitals of the Ti^{4+} cations [23]. These charge carriers present high reactive activity and can act with different paths. One is the recombination of electron-hole pairs without taking part in the degradation. The other involves gathering at the surface, and reacting with the pollutant [24]. In comparison, all of the spectra show similar curve shapes without new spectrum phenomena. Although the solidification pathway is modified, no notable shift to longer or shorter wavelengths was observed in the TiO_2-12-30 and TiO_2-20-30 coatings. Perhaps the main reason for this is that the rutile phase still dominates in both coatings, though the anatase content increases.

The photocatalytic performances are shown in Figure 5. All coatings present different degrees of activity in decomposing methylene blue with the irritation of UV light. The coating of TiO_2-12-0 shows depressed photocatalytic activity. This is consistent with other works [12,13]. Without modifying the solidification pathway, the anatase content in this coating is as low as 4%. For the TiO_2-12-30 and TiO_2-20-30 coatings, they both exhibit a significant increase in photocatalytic activity. Obviously, the enhanced activity is ascribed to the augmented anatase content in both TiO_2 coatings because they present similar structure. As the TiO_2-20-30 coating has a higher anatase content than TiO_2-12-30, it presents higher activity.

Furthermore, the variation in MB concentration with irradiation time is coincident with Langmuir-Hinshelwood model. The kinetics equation can be depicted by $-\ln C/C_0 = kt$, where C and C_0 are the measured concentration of MB and the initial concentration, respectively, and k is the time constant of the activity (h^{-1}). By a first-order fitting of the exponential term to the time t, the values of k are obtained for all coatings and summarized in Table 2. As presented in Table 2, the k value for the TiO_2-12-30 or TiO_2-20-30 coating is higher than that of the TiO_2-12-0 coating, as the former is

deposited with the modification of the solidification pathway. As clarified by the equation, the bigger value of *k* implies a higher photocatalytic activity.
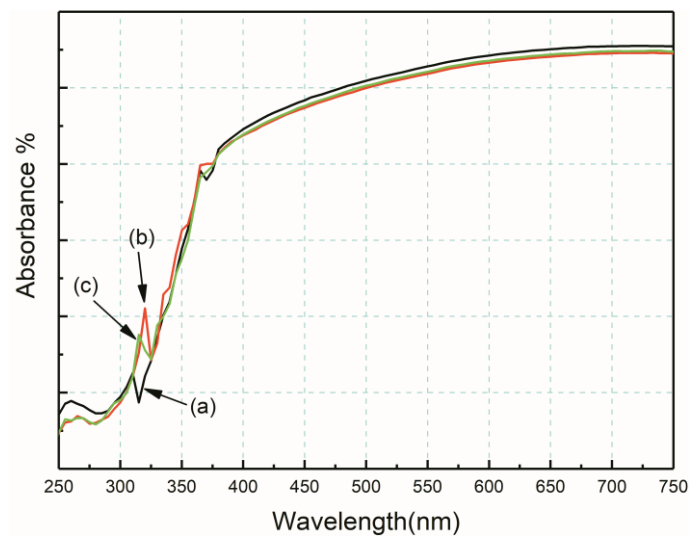

Figure 4. UV-Vis reflectance spectra of TiO_2 coatings: (**a**) TiO_2-12-0, (**b**) TiO_2-12-30, and (**c**) TiO_2-20-30.
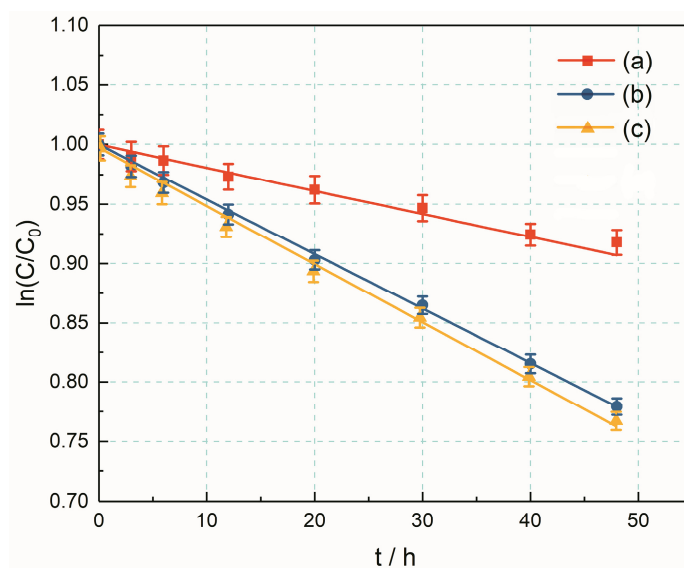
Figure 5. Photocatalytic activity in decomposing methylene blue of TiO_2 coatings: (**a**) TiO_2-12-0, (**b**) TiO_2-12-30, and (**c**) TiO_2-20-30.

4. Conclusions

Distilled water was injected into the plasma jet to modify the solidification pathway of inflight melted TiO_2 particles rather than adjusting the spray conditions. Results showed that the anatase phase was nucleated from melted TiO_2 particles under a high cooling rate due to its lower surface energy comparing to the rutile phase, and photocatalytic TiO_2 coatings with enhanced activity were obtained. Finally, the anatase content in TiO_2 coatings was augmented to 19.9% from 4%, and the time constant of the activity was increased to $0.0046 \, h^{-1}$ from $0.0017 \, h^{-1}$. In addition, the modification of the solidification pathway did not remarkably cause the loss of coating microhardness.

Author Contributions: Kui Wen, Xuezhang Liu and Kesong Zhou conceived and designed the experiments; Kui Wen and Xuezhang Liu performed the experiments; Kui Wen, Xuezhang Liu, Min Liu and Chunming Deng analyzed the data; Xuezhang Liu and Kui Wen wrote and revised the paper respectively.

Conflicts of Interest: The authors declare no conflict of interest.

References

1. Priyanka, K.P.; Revathy, V.R.; Rosmin, P.; Thrivedu, B.; Elsa, K.M.; Nimmymol, J.; Balakrishna, K.M.; Varghese, T. Influence of La doping on structural and optical properties of TiO_2 nanocrystals. *Mater. Charact.* **2016**, *113*, 144–151. [CrossRef]

2. Daram, P.; Banjongprasert, C.; Thongsuwan, W.; Jiansirisomboon, S. Microstructure and photocatalytic activities of thermal sprayed titanium dioxide/carbon nanotubes composite coatings. *Surf. Coat. Technol.* **2016**, *306*, 290–294. [CrossRef]

3. Zelekew, O.A.; Kuo, D.-H.; Yassin, J.M.; Ahmed, K.E.; Abdullah, H. Synthesis of efficient silica supported TiO_2/Ag_2O heterostructured catalyst with enhanced photocatalytic performance. *Appl. Surf. Sci.* **2017**, *410*, 454–463. [CrossRef]

4. Chung, L.; Chen, W.F.; Koshy, P.; Sorrell, C.C. Effect of Ce-doping on the photocatalytic performance of TiO_2 thin films. *Mater. Chem. Phys.* **2017**, *197*, 236–239. [CrossRef]

5. Cravanzola, S.; Jain, S.M.; Cesano, F.; Damin, A.; Scarano, D. Development of multifunctional TiO_2/MWCNT hybrid composite grafted on stainless-steel grating. *RSC Adv.* **2015**, *5*, 103255–103264. [CrossRef]

6. Quesada-Gonzalez, M.; Boscher, N.D.; Carmalt, C.J.; Parkin, I.P. Interstitial boron-doped TiO_2 thin films: The significant effect of boron on TiO_2 coatings grown by atmospheric pressure chemical vapor deposition. *ACS Appl. Mater. Interfaces* **2016**, *8*, 25024–25029. [CrossRef] [PubMed]

7. Taherniya, A.; Raoufi, D. The annealing temperature dependence of anatase TiO_2 thin films prepared by the electron-beam evaporation method. *Semicond. Sci. Technol.* **2016**, *31*, 125012. [CrossRef]

8. Chava, R.K.; Lee, W.M.; Oh, S.Y.; Jeong, K.U.; Yu, Y.T. Improvement in light harvesting and device performance of dye sensitized solar cells using electrophoretic deposited hollow TiO_2 NPs scattering layer. *Sol. Energy Mater. Sol. Cells* **2017**, *161*, 255–262. [CrossRef]

9. Liu, C.F.; Huang, C.P.; Hu, C.C.; Juang, Y.J. Photoelectrochemical degradation of dye wastewater on TiO_2-coated titanium electrode prepared by electrophoretic deposition. *Sep. Purif. Technol.* **2016**, *165*, 145–153. [CrossRef]

10. Anitha, V.S.; Lekshmy, S.S.; Joy, K. Effect of annealing on the structural, optical, electrical and photocatalytic activity of ZrO_2-TiO_2 nanocomposite thin films prepared by sol-gel dip coating technique. *J. Mater. Sci. Mater. Electron.* **2017**, *28*, 10541–10554. [CrossRef]

11. Mauer, G.; Guignard, A.; Vaßen, R. Plasma spraying of efficient photoactive TiO_2 coatings. *Surf. Coat. Technol.* **2013**, *220*, 40–43. [CrossRef]

12. Bozorgtabar, M.; Rahimipour, M.; Salehi, M.; Jafarpour, M. Structure and photocatalytic activity of TiO_2 coatings deposited by atmospheric plasma spraying. *Surf. Coat. Technol.* **2011**, *205*, S229–S231. [CrossRef]

13. Colmenares-Angulo, J.; Zhao, S.; Young, C.; Orlov, A. The effects of thermal spray technique and post-deposition treatment on the photocatalytic activity of TiO_2 coatings. *Surf. Coat. Technol.* **2009**, *204*, 423–427. [CrossRef]

14. Ctibor, P.; Seshadri, R.C.; Henych, J.; Nehasil, V.; Pala, Z.; Kotlan, J. Photocatalytic and electrochemical properties of single- and multi-layer sub-stoichiometric titanium oxide coatings prepared by atmospheric plasma spraying. *J. Adv. Ceram.* **2016**, *5*, 126–136. [CrossRef]

15. Zhang, J.; Zhao, Z.; Wang, X.; Yu, T.; Guan, J.; Yu, Z.; Li, Z.; Zou, Z. Increasing the oxygen vacancy density on the TiO_2 surface by La-doping for dye-sensitized solar cells. *J. Phys. Chem. C* **2010**, *114*, 18396–18400. [CrossRef]

16. Rajender, G.; Giri, P.K. Strain induced phase formation, microstructural evolution and bandgap narrowing in strained TiO_2 nanocrystals grown by ball milling. *J. Alloy. Compd.* **2016**, *676*, 591–600. [CrossRef]

17. Berger-Keller, N.; Bertrand, G.; Filiatre, C.; Meunier, C.; Coddet, C. Microstructure of plasma-sprayed titania coatings deposited from spray-dried powder. *Surf. Coat. Technol.* **2003**, *168*, 281–290. [CrossRef]

18. Chen, D.; Jordan, E.H.; Gell, M. Porous TiO_2 coating using the solution precursor plasma spray process. *Surf. Coat. Technol.* **2008**, *202*, 6113–6119. [CrossRef]

19. Shen, P.K.; He, C.; Chang, S.; Huang, X.; Tian, Z. Magnéli phase Ti8O15 nanowires as conductive carbon-free energy materials to enhance the electrochemical activity of palladium nanoparticles for direct ethanol oxidation. *J. Mater. Chem. A* **2015**, *3*, 14416–14423. [CrossRef]

20. Dosta, S.; Robotti, M.; Garcia-Segura, S.; Brillas, E.; Cano, I.G.; Guilemany, J.M. Influence of atmospheric plasma spraying on the solar photoelectro-catalytic properties of TiO_2 coatings. *Appl. Catal. B Environ.* **2016**, *189*, 151–159. [CrossRef]

21. Hanaor, D.A.H.; Sorrell, C.C. Review of the anatase to rutile phase transformation. *J. Mater. Sci.* **2011**, *46*, 855–874. [CrossRef]

22. Cizek, J.; Khor, K.A.; Dlouhy, I. In-flight temperature and velocity of powder particles of plasma-sprayed TiO_2. *J. Therm. Spray Technol.* **2013**, *22*, 1320–1327. [CrossRef]

23. Carneiro, J.O.; Azevedo, S.; Fernandes, F.; Freitas, E.; Pereira, M.; Tavares, C.J.; Lanceros-Méndez, S.; Teixeira, V. Synthesis of iron-doped TiO_2 nanoparticles by ball-milling process: The influence of process parameters on the structural, optical, magnetic, and photocatalytic properties. *J. Mater. Sci.* **2014**, *49*, 7476–7488. [CrossRef]

24. Toma, F.-L.; Berger, L.-M.; Shakhverdova, I.; Leupolt, B.; Potthoff, A.; Oelschlägel, K.; Meissner, T.; Gomez, J.A.I.; De Miguel, Y. Parameters influencing the photocatalytic activity of suspension-sprayed TiO_2 coatings. *J. Therm. Spray Technol.* **2014**, *23*, 1037–1053. [CrossRef]